Global-scale hybrid simulation of cusp precipitating ions associated with magnetopause reconnection under southward IMF

B. Tan,[1] Y. Lin,[1] J. D. Perez,[1] and X. Y. Wang[1]

Received 12 June 2011; revised 19 December 2011; accepted 23 January 2012; published 14 March 2012.

[1] With a 3-D global-scale hybrid simulation model, we investigate the energy spectra of cusp precipitating ions and issues associated with magnetopause reconnection under a southward IMF. Both the spatial and temporal energy spectra of cusp precipitating ions are computed by tracing trajectories of the transmitted magnetosheath ions. The spatial spectrum shows a dispersive feature consistent with satellite observations, with higher energy particles at lower latitudes and lower energy particles at higher latitudes. The simulation reveals (1) how and where particles are transmitted from the solar wind into the magnetosphere via direct magnetic reconnection on the dayside; (2) how the features of the spectra are related to ongoing magnetic FTEs; and (3) how the motion of the cusp, particularly the latitudinal variation of the open/closed field line boundary, is correlated with the dayside reconnection and reflected in the energy flux spectra of the precipitating ions as a function of time.

Citation: Tan, B., Y. Lin, J. D. Perez, and X. Y. Wang (2012), Global-scale hybrid simulation of cusp precipitating ions associated with magnetopause reconnection under southward IMF, *J. Geophys. Res.*, *117*, A03217, doi:10.1029/2011JA016871.

1. Introduction

[2] The dayside cusp is the region of the Earth's magnetosphere where downward precipitating ions reflect magnetic reconnection at the magnetopause. The precipitating cusp particles as observed by satellites inside the magnetosphere often show an energy-latitude dispersion, i.e., decreasing energy with increasing latitude [*Rosenbauer et al.*, 1975; *Reiff et al.*, 1977]. The observed, dispersive structure exhibits "stepped" ion signatures with variations in flux levels and sudden changes in the energy [*Newell et al.*, 1991]. Two-dimensional models have associated the observed dispersive energy spectra [*Onsager et al.*, 1993; *Lockwood et al.*, 1994] with ongoing magnetic reconnection at the magnetopause. Statistical analysis of many events shows that the cusp precipitation depends on the magnetopause merging rate in both quantitative and qualitative ways [*Newell et al.*, 2007]. Although researchers have made a lot of efforts to understand them, in some cases ambiguity cannot be eliminated in the interpretation of observed energy spectra of precipitating ions because of limited spatial coverage of spacecrafts [*Onsager et al.*, 1995; *Trattner et al.*, 2007]. Thus, a simulation study provides a new perspective as it shows direct and clear connection between the large scale magnetic field configuration and local structures of the cusp ion signatures due to magnetopause reconnection.

[3] In our previous work [*Tan et al.*, 2011, hereinafter paper 1], we presented a numerical simulation of dayside magnetic reconnection with the dipole tilt angle of the Earth equal to 15°. That result is hereafter referred to as case 1, where the interplanetary magnetic field (IMF) is purely southward. A three-dimensional (3-D) global-scale hybrid model was utilized in case 1, in which the fully kinetic ion physics is solved in the self-consistent electromagnetic field. In this paper, we analyze the precipitating ions in the cusp region from case 1. In section 2, we briefly describe the simulation model, and the results are presented in section 3, followed by a summary in section 4.

2. Simulation Model

[4] We adopt the global-scale hybrid simulation scheme described by *Swift* [1996] and implemented by *Lin and Wang* [2005] for 3-D simulations of the dayside magnetosphere. The ions are advanced by their equation of motion, the electric field is determined by the electron momentum equation, while the magnetic field is updated by Faraday's law. The simulation model as well as parameters are the same as case 1 of paper 1.

[5] In the following presentation, spherical coordinates are used in the GSM system. The polar angle θ measures from the positive GSM z axis. The magnetic field B is scaled by the IMF B_0; the ion number density N by the solar wind density N_0; the time t by the inverse of the ion gyrofrequency (Ω_0^{-1}); the flow velocity V by the Alfvén velocity in the solar wind V_{A0}; the pressure by $N_0 V_{A0}^2$ and the energy by $E_0 = V_{A0}^2$. The ion inertial length in the solar wind $\lambda_0 = \frac{c}{\omega_{pi0}}$ is set to be 0.1 in the simulation unit. Note that c is the speed of light, and ω_{pi0} is the ion plasma frequency in the solar wind. The length is expressed in unit of Earth radius ($1R_E$ = 6378

[1]Physics Department, Auburn University, Auburn, Alabama, USA.

0148-0227/12/2011JA016871

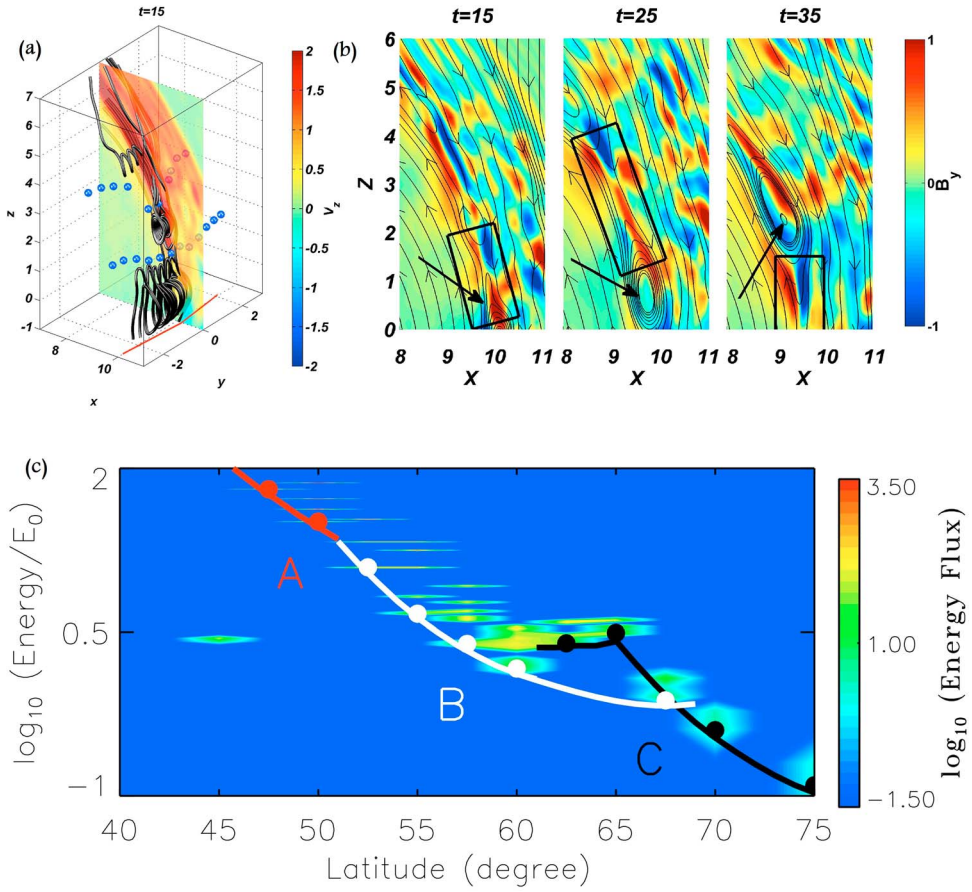

Figure 1. (a) The 3-D plot shows reconnection X lines in blue dots and red line segment at $t = 15$ with the z component of ion bulk flow V_z contours in the noon meridian plane. (b) The contours show B_y component in the noon meridian planes and projected magnetic field lines at $t = 15$, 25, 35, respectively. (c) Spatial energy spectrum of cusp precipitating ions in the logarithmic scale showing a dispersive feature. The red, white, and black dots indicate energies of some typical ions at the minimum-energy cutoff energies of parts A, B, and C, respectively, which are related to three reconnection events.

kilometers) and the energy flux in $\frac{E_0 V_{A0}}{R_E^3}$. The Alfvén speed in the solar wind V_{A0} is equal to $0.1 R_E \Omega_0$.

[6] The simulation domain contains the dayside region with GSM $x > 0$ and a geocentric distance $4 \le r \le 24.5\ R_E$. Free boundary conditions are utilized at $x = 0$ during the simulation. Inflow boundary conditions of the solar wind are applied at $r = 24.5\ R_E$. The inner boundary at $r = 4\ R_E$ is perfectly conducting.

[7] Initially, a geomagnetic dipole field tilted sunward by 15° is centered at $r = 0$, along with an image dipole and a purely southward IMF of $B_z = -1$. Thus the northern cusp region is well within the simulation domain. The solar wind flows into the system along the $-x$ direction with an isotropic drifting-Maxwellian distribution. A current-dependent collision frequency, $\nu \simeq 0.01 \Omega J / J_0$, is imposed in the simulation, where $J_0 = B_0 / \mu_0 \lambda_0$. Note that J is the current density.

[8] We choose a uniform solar wind with $\beta_i = \beta_e = 0.5$ and an Alfvén Mach number $M_A = 5$. Non-uniform grid spacing is used, and the finest grid spacing in the radial direction ($\Delta r = 0.088 R_E$) is located near $r = 10 R_E$ so that a higher resolution is produced near the magnetopause. A grid with $160 \times 104 \times 130$ cells is used.

3. Simulation Results

3.1. Reconnection Events and Spatial Energy Spectrum

[9] As the solar wind ions convect carrying the IMF, the bow shock, magnetosheath, and magnetopause form in a self-consistent manner around $t = 10$. The reconnection events discussed in paper 1 and this paper are identified by the connectivity change of magnetic field lines as well as other supporting evidence, which is discussed in detail in paper 1.

[10] Figures 1a and 1b are similar to Figure 3 in paper 1, which illustrates the magnetic field configuration around the magnetopause in the northern hemisphere before $t = 40$. The left 3-D plot (Figure 1a) shows the magnetic field configuration at $t = 15$. The black lines are magnetic field lines. Note that the magnetic field lines are approximately symmetric about the noon meridian plane. There are two X-line segments shown as in blue dots, where the term "X line" is defined as the intersection of two surfaces that separate distinct field lines of four different local regions (earthward

side of the magnetopause current sheet, sunward side of the current sheet, from the sunward side to the earthward side, and from the earthward side to the sunward side following the magnetic field direction). Under the purely southward IMF, X line segments are approximately parallel to the equatorial plane along the dayside magnetopause.

[11] In addition to the two X lines illustrated by blue dots, there is a third X line at $z = -1$, as illustrated by red line segments in Figure 1a, which is not shown in Figure 3 of paper 1. The reconnection events that we will discuss in this paper are associated with these three X lines.

[12] Figure 1b corresponds to B_y components in the noon meridian plane at t = 15, 25, and 35. The black lines are projected field lines. The boundary region with a large field rotation of about 180° is the magnetopause. The arrows indicate the same northward moving flux rope which is shown at the lowest z in Figure 1a.

[13] Figure 1c shows the spatial variation at fixed time of the energy flux spectrum of the precipitating transmitted magnetosheath ions from case 1 during the magnetopause reconnection. The horizontal axis plots the latitude, which is related to the spherical polar angle θ by $Latitude = 90 - \theta$. The spatial spectrum is obtained from near field-aligned particles with pitch angle less than 10.0° for $r = 7.5\ R_E$ and t = 40, in order to model the field aligned ion flux. The energy gaps at constant latitudes in the energy spectrum are due to the limited number of "particles" with pitch angle less than 10.0° at the position where ion fluxes are recorded. Note that the number of ion particles per grid cell are varied from 100 to 500 in the simulation.

[14] The energy flux is recorded at discrete latitudes of 2.5° increments, from 40.0° to 75.0°, which causes the blobs of enhanced ion fluxes at the plotted center latitudes. The ion flux enhancement at 45.0° latitude is associated with particles on the Earth's dipole field lines in the simulation. Since it is not related to the magnetic reconnection process, we will omit it in the following discussion.

[15] It is found that three parts of the spectrum, A, B, and C, shown in Figure 1c, are related to the entrance areas of the cusp precipitating particles associated with the three reconnection X lines on the magnetopause as shown in Figure 1a. The three parts of the spectrum are indicated with three lines along the minimum-energy cutoff in Figure 1c, i.e., the minimum energy at each latitude in the spatial spectrum. The red, white, and black dots indicate energies of some typical ions at the minimum-energy cutoff energies of parts A, B, and C, respectively. To interpret observation data, the low-velocity cutoff has been used to infer the reconnection sites on the magnetopause [*Trattner et al.*, 2007] by tracing particles at the minimum-energy cutoff back along the magnetic field lines. Overall, the resulting particle spectrum in each of the three parts replicates the dispersive features in spacecraft data under similar IMF conditions [*Onsager et al.*, 1995], i.e., that shows higher energy particles at lower latitudes and lower energy particles at higher latitudes. Of particular interest is the overlap and "step" between the minimum-energy cutoff parts B and C in the spectrum, between latitudes 60°–70°.

3.2. Precipitating Ions at the Minimum-Energy Cutoff

[16] In this subsection, we explain how and where precipitating ions at the minimum-energy cutoff are transmitted from the solar wind into the magnetosphere via direct magnetic reconnection related to the three X lines shown in Figure 1, by tracing trajectories of the ions at the minimum-energy cutoff [*Wang et al.*, 2009]. Note that all the traced ions originate from the magnetosheath. One reconnection region is associated with the X line shown in the red line segments, which we will refer to as region A because it is the source region of the ions at the minimum-energy cutoff in part A of the spectrum we show in Figure 1. Similarly, ions at the minimum-energy cutoff in part B of the spectrum come from the reconnection region associated with the X line in the blue dots at the middle latitudes in Figure 1. This region is denoted as region B. As for ions at the minimum-energy cutoff in part C of the spectrum, they are found to be from reconnection region associated with the X line in blue dots at the higher latitudes in Figure 1, which is referred as region C.

[17] In the following subsections, we describe magnetic reconnection in each region as well as its impact on the spatial spectrum shown in Figure 1 and explain how the particles at the minimum-energy cutoff accelerate and decelerate during the process.

3.2.1. Precipitating Ions at the Minimum-Energy Cutoff Associated With Region A

[18] Figure 2 shows in the particle trajectories of two particles, the red and gray balls, at the minimum-energy cutoff from reconnection in region A seen in Figure 1c, which possess the highest final energies among all the particles at the minimum-energy cutoff in the spectrum at t = 40. Note that the red ball marks the current position of the particle that reaches the lowest latitudes of 47.5° at t = 40, and the gray ball for the particle that reaches 50°. The black balls indicate the final positions for the two particle. The trajectories are colored tubes coded linearly with the kinetic energies of the precipitating ions from t = 0 to t = 40 with a time step of δt = 0.25. Since kinetic energy varies along the trajectory as a function of time, the color of the trajectory varies correspondingly. The starting positions of particles are marked with a star. The kink in the particle trajectory that is the closest to the final position, marked with a yellow pyramid, is where the corresponding particle enters across the magnetopause from the magnetosheath due to magnetic reconnection. The entry region of these particles is localized near the noon-midnight meridian plane. The black field lines illustrate the magnetic field configuration near the two particles at t = 5, 25, 35, and 40. In Figure 2 (top left), the particle indicated with a red ball is the "red curve" particle in Figure 3. The contours show the ion density at the corresponding time in the noon meridian and equatorial planes. The particle ending at the latitude of 47.5° has a final kinetic energy of $64.3E_0$ while that ending at the latitude of 50° has a final kinetic energy of $32.4E_0$. Note that an ion possessing a speed of $|V_{A0}|$ has a kinetic energy of 0.5 in the simulation units, with the formula $E = \frac{1}{2}mV^2$ used.

[19] At t = 5, i.e., before the reconnection is initiated, both particles are on magnetosheath field lines, as shown in Figure 2 (top left). The red curve in Figure 3 shows the total speed of the precipitating ion at the minimum-energy cutoff that ends at the latitude 47.5° in Figure 1, not only the parallel speed, as a function of time for typical precipitating ions associated with the reconnection in region A. As

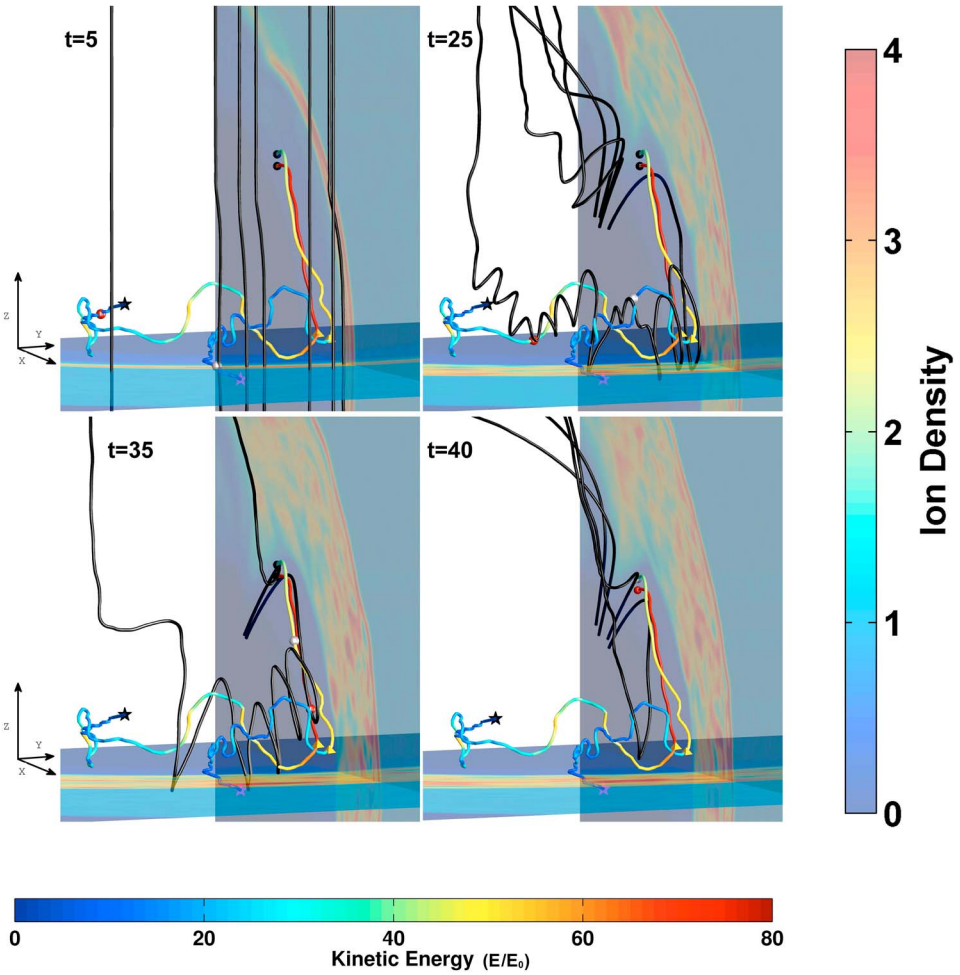

Figure 2. The trajectories in colored tubes of particles at the minimum-energy cutoff from region A and the magnetic field configuration in black lines at (top left) $t = 5$, (top right) 25, (bottom left) 35, and (bottom right) 40 in the GSM system. Axis direction is shown in the left of either row. The trajectories are color-coded with their current kinetic energies with the starting points indicated by colored stars. The particle indicated by a red ball in Figure 2 (top left) corresponds to the "red curve" particle in Figure 3, of which the trajectory starts with a black star. Starting from 47.5°, particles at minimum-energy latitude in the part A of spectrum have final energies of $64.3E_0$ and $32.4E_0$, respectively. Also shown are the contours of ion density N.

indicated by the y axis label, the speed is scaled to the magnitude of Alfvén velocity in the solar wind, i.e., $|V_{A0}|$. The "red" curve particle has an average speed of $v_p \sim 4.5$ around $t = 5$ before entering the magnetopause boundary layer. The particle is then accelerated to the $\frac{\mathbf{E}\times\mathbf{B}}{B^2}$ speed. The acceleration is caused by the $\mathbf{E} \times \mathbf{B}$ motion, where the reconnection electric field $\mathbf{E} = -\mathbf{V_e} \times \mathbf{B}$ is nearly in the $+y$ direction, and B is mostly in the $-\hat{\mathbf{r}}$ where $\hat{\mathbf{r}}$ is the radial direction. Note that E_y is the reconnection electric field that is enhanced only in the reconnection layer. When the particle moves out of the magnetopause boundary layer, E_y decreases.

[20] From $t = 11$ to $t = 16$, the "red" curve particle is slightly accelerated to $v_p \sim 7$ while being trapped in the reconnected flux rope shown in Figure 2 (top right). The flux rope forms between the two X lines. Note that the two X lines have moved northward, compared to their location at $t = 15$ shown in Figure 1b.

[21] The "red curve" particle is then gradually accelerated to $v_p \sim 12.5$ at $t \simeq 35$, as seen in Figure 3. At this moment, it has just passed the entry point on the magnetopause, as marked by the yellow pyramid in Figure 2. The entry point is just north of the X line that is shown in Figure 1 as red line segments. From $t = 10$ to $t = 35$, the speed enhancement of the "red curve" particle is, comparable to twice the local magnetosheath Alfvén speed $V_A \sim 2.3V_{A0}$ while reconnected field lines convect northward with an average speed comparable to $\sim V_A$, as expected for acceleration in Alfvén type large-amplitude waves in magnetic reconnection [*Lin and Lee*, 1994].

[22] From $t = 35$ to $t = 37.5$, the particle is at nearly the same speed while traveling in the boundary layer toward high latitudes. After that, it was field-aligned and slightly decelerated to $v_p \sim 11.4$ in the magnetosphere (on the earthward side of the boundary layer). The deceleration occurs when the particle exits the reconnection exhaust layer

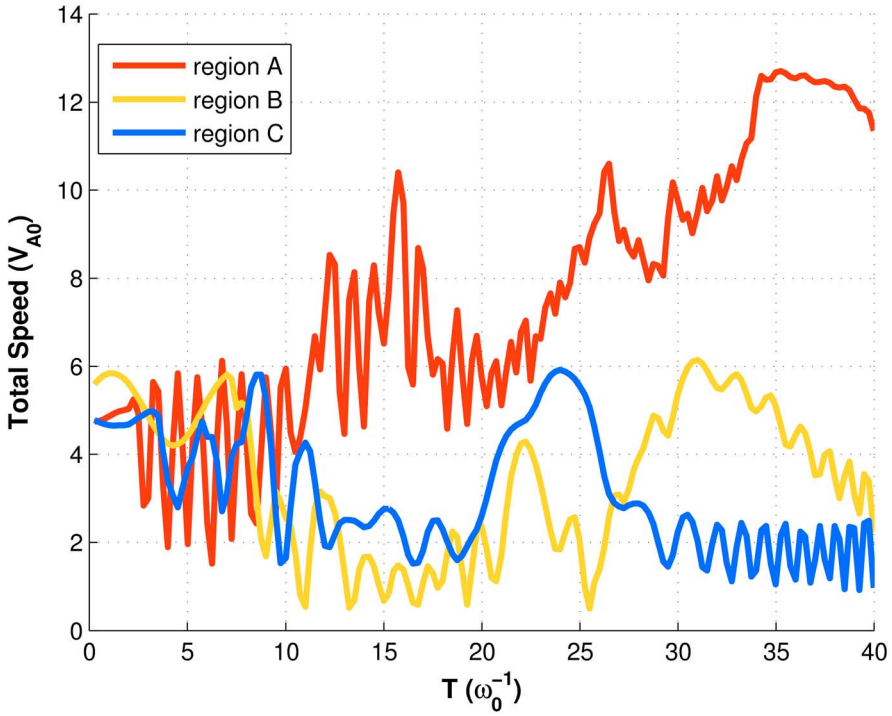

Figure 3. Particle speed as a function of time for typical ions associated with reconnection A, B, and C, shown by the red, yellow, and blue curves.

and enters into the magnetosphere and inside the cusp where B increases.

[23] The average speed of this "red curve" particle after the entry point at $t = 34$ is about 12.3, which is larger than the average speed of 9.3 for the other particle of region A at the minimum-energy cutoff ending at the latitude of 50°. The particle ending at the latitude of 50° enters the magnetopause at $t \simeq 31$, earlier than the particle ending at the latitude of 47.5°. A longer time of flight for the slower particle compensates an energy difference of $31.9E_0$, which is consistent with the time of flight or velocity filter effect suggested by *Shelley et al.* [1976] and *Reiff et al.* [1977]. Note that only particles moving with a positive parallel velocity relative to the poleward convecting field lines can enter the magnetosphere, which should lead to a D-shaped ion velocity distribution of the transmitted magnetosheath ions if the field line convects with a constant speed, as in quasi-steady reconnection [*Cowley*, 1982; *Tan et al.*, 2011].

[24] Figure 4 shows how the "red curve" particle (red) ending at the latitude of 47.5° reaches its final position in the cusp, compared with the particle ending at the latitude of 50° (light red). Let times $t = t_1 < t_2 < t_3$, while $t_3 = 40$ is the final instant when the particles reach $r = 7.5\ R_E$. For the reconnection in region A at the lowest latitude near the subsolar area, the X line remains nearly at the same location. The fact that the field line associated with the "red" particle is located at a lower latitude indicates that this field line reconnects later than the field line associated with the "light red" particle, and thus has convected a shorter time on the magnetopause from the same X line. Since the transmitted

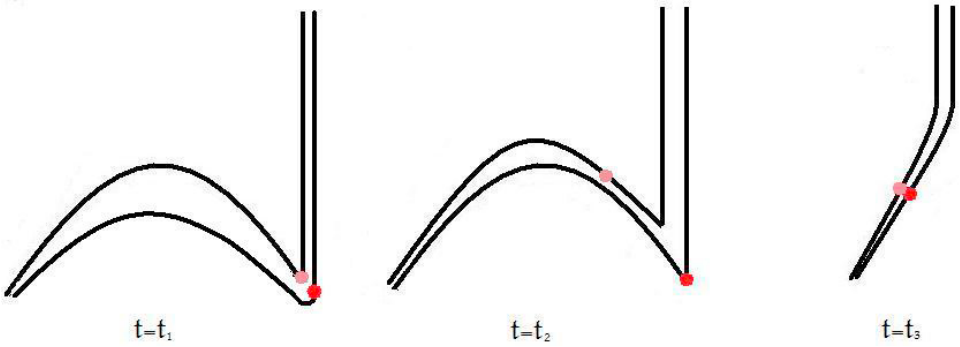

Figure 4. Schematic diagram shows how the "red curve" particle (red) ending at the latitude of 47.5° reaches its final position in the cusp at $t = t_1$, $t = t_2$, $t = t_3$ ($t_1 < t_2 < t_3$), compared with the particle ending at the latitude of 50° (light red).

particles ending at the same latitudinal location in Figure 1 are located nearly on the same field line as the field line convects poleward, the one at the minimum-energy cutoff tends to enter the magnetopause nearest the X line (instead of from a higher latitude when the opened field line has convected a certain distance), corresponding to the longest travel time. Both the "red" and the "light red" particles at the minimum-energy cutoff in Figure 4 enter the magnetosphere around the same location, while the "red" particle enters later and travels a shorter time. Since the length of their effective paths are approximately equal, the "red" ("light red") particle must have a higher (lower) energy, as seen in the hybrid simulation. The "light red" particle enters the magnetosphere from the reconnection site near the subsolar area at $t = t_1 = 31$, ahead of the "red" particle. When the "red" particle enters the magnetosphere at $t = t_2 = 34$, the "light red" particle has moved northward on an open field line. In the end, both particles arrive at the final altitude in the cusp at $t = t_3 = 40$.

[25] It is worthy noting that Figure 4 sketches much simplified processes, whereas in the 3-D simulation the field lines are helical, and the particles are trapped in the flux ropes before passing the entry point into the magnetosphere. The particle ending at the latitude of 47.5° (the "red curve" particle in Figure 3) stays inside the boundary layer for an extended time and experiences several energizations at times $t \simeq 15$, 25, and 33 as it travels along the flux rope, which are probably associated with multiple X-line segments of limited length and help lift the particle up to a higher energy level before the final kink. On the other hand, the particle ending at the latitude of 50.0° has gained less energy before $t = 25$ when it reaches the entry point, as indicated by the color of its trajectory. The energization history of the two particles contributes a large part to the energy difference of the two particles in the cusp.

3.2.2. Precipitating Ions at the Minimum-Energy Cutoff Associated With Region B

[26] In this subsection, we discuss the precipitating ions at the minimum-energy cutoff associated with region B for which the trajectories are shown in Figure 5. The format of Figure 5 is similar to Figure 2, except that the trajectories are color coded with the final energy of each particle. Particles precipitating at these latitudes have been accelerated at the middle latitudes in the pre-noon flank of the magnetopause. The ion ending at the latitude of 57.5° and associated with reconnection B is used as an example to illustrate how the precipitating ions at the minimum-energy cutoff associated with region B enter the magnetopause and reach their final positions. The speed is shown as the "yellow curve" in Figure 3. In Figure 5 (top left), the location of the "yellow curve" particle is associated with the light blue trajectory and has been marked with a black arrow.

[27] At $t = 5$, all the particles are on magnetosheath field lines, shown in Figure 5 (top left). As shown in Figure 3, the "yellow curve" ion has an initial speed about the same as that of the "red curve" particle from region A. Different from the "red curve" particle, the "yellow curve" particle is originally moving tailward with the magnetosheath bulk flow but then dragged sunward by a reconnected field line on the flank side of the magnetopause, resulting in a deceleration at $t \simeq 10$, as shown in Figure 3.

[28] The "yellow curve" particle in Figure 3 enters the magnetopause at $t \simeq 25$ and is then accelerated. The acceleration near the final kink (yellow pyramid) for this particle from $t = 25.5$ to $t = 31$ is mildly smaller than that for the "red curve" particle from $t = 33$ to $t = 34.5$, as indicated by Figure 3. Although the "yellow curve" particle gains a similar energy as the "red curve particle" at their final kinks through reconnection, the "yellow curve" particle reaches a peak $v_p \sim 6$ around $t \simeq 31$ as seen in Figure 3, a speed that is much less than that of the "red curve" particle. This difference can be explained by their energization history in Regions A and B. First, the "yellow curve" particle experience less energizations than the "red curve" particle before the final kink. Secondly, unlike the "red curve" particle, the "yellow curve" particle has a velocity component in the $-y$ direction before it reaches the reconnection layer, which is indicated by its trajectory in Figure 5. Then the "yellow curve" particle experiences a deceleration and is seen move out the boundary layer quickly.

[29] Overall, a long flux tube tends to exist in the subsolar reconnection region (Region A) and thus a long energization history contributes to the latitudinal dispersion between part A and part B of the spectrum. On the other hand, the mechanism of the dispersive minimum-energy cutoff within part B appears to be different from that within part A. The particles at the minimum-energy cutoff enter from region B of the magnetopause reconnection with a smaller average speed of ~ 4.4, compared to the average speed of 10.8 for part A. The standard deviation of the average speeds for region B is ~ 0.7, compared with the standard deviation of ~ 2.1 for region A. Thus, the difference in energies at the entry points for region B is not enough to account for the latitudinal separation in the corresponding cusp spectrum. Rather, particles ending at different latitudes over the spectral range enter the magnetosphere at different times ranging from $t = 15$ to $t = 31$, as the X line moves poleward and antisunward, and thus the entry points of particles appear to have shifted accordingly. Note that the X line corresponding to region A is located near the equator, of which the poleward movement is less significant than that for the X line of region B.

[30] In this region, particles precipitating at lower latitudes enter the magnetopause at later times so that by $t = 40$ the corresponding field lines have convected shorter latitudinal distances. The energies of these particles, therefore, must be higher in order to reach the same cusp altitude within the shorter time intervals. Moreover, the foot point of the latest-reconnected field line shifts equatorward with time due to the erosion of magnetospheric field lines at the low latitudes under the purely southward IMF as we will show in Figure 6, which also contributes to the appearance of higher minimum-energy cutoff at lower latitudes.

3.2.3. Precipitating Ions at the Minimum-Energy Cutoff Associated With Region C

[31] Particles associated with reconnection region C have entry points localized in the pre-noon flank of the high-latitude magnetopause. The trajectories for the precipitating ions at the minimum-energy cutoff from region C are not shown because they are similar to those from region B. The typical speed change is shown in Figure 3 as the blue curve, which corresponds to the particle that reaches a final position at the latitude of 70°.

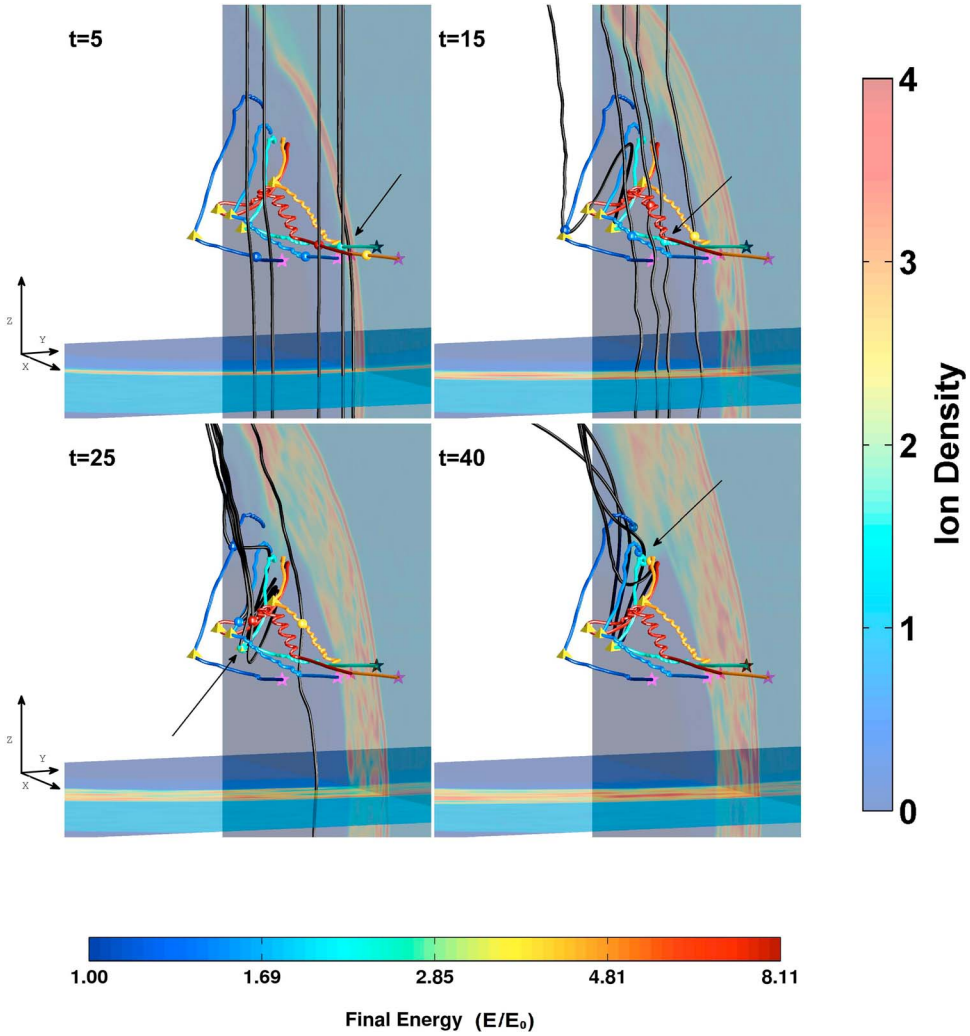

Figure 5. The trajectories in colored tubes of particles at the minimum-energy cutoff from region B and the magnetic field configuration in black lines at (top left) t = 5, (top right) 25, (bottom left) 35, and (bottom right) 40 in the GSM system. Axis direction is shown in the left of either row. The trajectories are color-coded with their final kinetic energies with the starting points indicated by the colored stars. The particle indicated by an black arrow in Figure 5 (top left) corresponds to the "yellow curve" particle in Figure 3, of which the trajectory starts with a black star. Starting from 52.5°, particles at minimum-energy latitude in the part B of spectrum have final energies of $12.37E_0$, $4.65E_0$, $2.47E_0$, $1.47E_0$ and $0.82E_0$, respectively. Also shown are the contours of ion density N.

[32] Similar to the "yellow curve" particle for region B, the "blue curve" particle also undergoes a deceleration and then acceleration in the magnetopause, followed by a final deceleration in the magnetosphere, as seen in Figure 3. The particles in region C of the spectrum are around the highest latitudes in the cusp. The field line convection speed becomes small in the cusp at the final position of the region C ions, where the radial distance is smaller, and the field lines are close to 90° geomagnetic latitude, compared to those at the dayside subsolar region. Thus the energy of the "blue" particle quickly drops back to its original value before the acceleration. The fact that three parts of the ion spectrum are associated with the three independent X line segments, explains the independence of each part of the spectrum. During the time dependent reconnection, time varying reconnection rate, different locations and extensions of the X line segment cause "energy plateaus" and an "energy step" between the three parts in the spectrum shown in Figure 1c.

3.3. Energy Flux Due to Precipitating Ions as a Function of Time

[33] For satellite observations, the energy spectrum is a combination of both spatial and temporal effects. In this section, we focus on the impact of the temporal effect on the energy spectrum of the cusp precipitation. Figure 6 (top) plots the energy spectrum as a function of time while our virtual satellite is stationary at the fixed location of $r = 7.5\ R_E$ and latitude of 52.5° in the noon meridian plane. The y axis is the particle energy on a logarithmic scale, while the color represents the energy flux levels, also on a logarithmic scale. The re-occurrence of precipitating ions and the trend of the

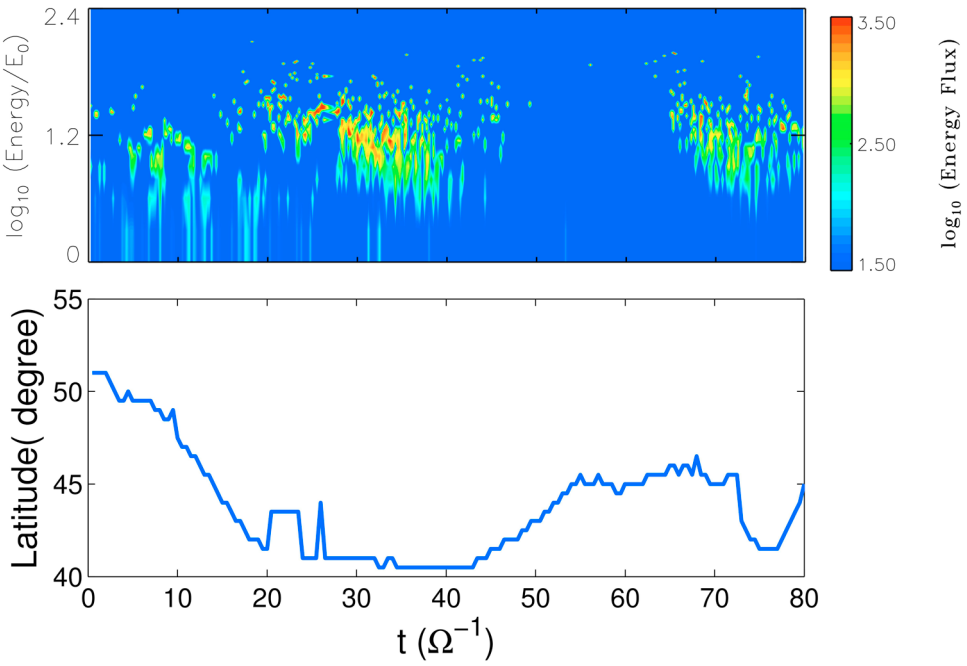

Figure 6. (top) Particle energy spectrum in the logarithmic scale as a function of time at a fixed position of $r = 7.5\ R_E$ and latitude of 52.5°. (bottom) Latitudinal position of the dayside open/close field boundary, at $r = 7.5\ R_E$, as a function of time. The equatorward (low-latitude) cusp is determined by the last open field line. Also note that the cusp width at $r = 7.5R_E$ is around 35°.

minimum-energy cutoff in the spectrum are found to be associated with the oscillation of the open/close field line boundary.

[34] Figure 6 (bottom) plots the latitudinal position of the dayside open/closed field line boundary in the noon meridian plane at $r = 7.5$ as a function of time, from $t = 0$ to $t = 80$. The equatorward (low-latitude) cusp is determined by the last open field line and related to magnetic reconnection at the lowest latitude (region A). It oscillates with time due to the time variation of the reconnection rate there. From $t = 15$ to $t = 40$, the probe location is well inside the cusp while the open/close field boundary is located at 41° latitude, and a continuous temporal spectrum of ion precipitation is observed. When the open/close field boundary of the low-latitude cusp moves to a higher latitude around $t = 50$, the ion precipitation becomes sparse and then disappears at the specific location.

[35] As seen from Figure 2, the particles are precipitating poleward of the open/close field line boundary of the cusp. The ion density contours show a cusp shape, and the equatorial (low-latitude) boundary of the "particle" cusp is located poleward to the equatorial boundary of the "field line" cusp. In other words, there is the deviation between the "particle" equatorial boundary and the "field line" equatorial boundary of the cusp. So the corresponding ion precipitation near the low-latitude boundary of the cusp moved to a location poleward to the virtual probe when the cusp moved poleward. Note that the latitudinal location of the ion precipitation is poleward of the last open/close field line due to the time-of-flight of particles while the field lines convect poleward. Also note that the cusp width at $r = 7.5R_E$ is around 35°. Later at $t = 70$, the field-aligned ion flux recurs as the open/close field boundary retreats to lower latitudes again.

[36] The minimum-energy cutoff at $t > 20$, after the formation of the bow shock, magnetosheath, and magnetopause, clearly trends down in the temporal spectrum when the open/closed field boundary of the cusp moves to lower latitudes, and up when the boundary moves to higher latitudes. Our simulation shows that as the subsolar reconnection (region A) gets weaker, which results in a high-latitude shift of the open/closed field boundary, the magnetopause reconnection is dominated by events at higher latitudes. As the reconnection site moves to the higher latitudes, it corresponds to a shorter time of flight for particles ending at the specific cusp latitude, leading to an increased minimum-energy cutoff of particles.

4. Summary

[37] In summary, cusp ion injections associated with magnetopause reconnection are investigated with a 3-D hybrid simulation. Under a purely southward IMF, both spatial and temporal energy spectra of cusp precipitating ions are obtained.

[38] The spatial spectrum of field-aligned particles at a constant geocentric radius and fixed time in the cusp replicates the observed energy dispersive feature of particles. Multiple parts of the spectrum, however, are found to be associated with multiple reconnection events at the dayside magnetopause. Both the multiple X-line reconnection with flux ropes and single-X line type reconnection events result in similar dispersive ion spectra.

[39] In the temporal energy spectrum recorded at a certain location, the occurrence and disappearance of ion

precipitation reflect the latitudinal oscillation of the open/closed field line boundary of the cusp. Data from satellite crossings of the cusp are expected to be a combination of the spatial and temporal effects.

[40] The simulations reported here show that the dispersive ion spectra of particles entering the cusp observed by satellites is more involved than the 2-D pictures based upon time of flight effects. It has been shown that (1) the reconnection responsible for the particle entry is neither steady in time nor localized in space; (2) the particle acceleration does not occur at a single point in space and time as the particle crosses a thin magnetopause distinguished by a kink in the field line, but is a much more involved process; and (3) different degrees of acceleration near the final entry points and the energization history of the particles contribute to the latitudinal energy dispersion.

[41] **Acknowledgments.** This work was supported by NASA grant NAG5-12899 and NSF grants ATM-0646442 and ATM-0852682 to Auburn University. Computer resources were provided by the Arctic Region Supercomputer Center.

[42] Masaki Fujimoto thanks the reviewers for their assistance in evaluating this paper.

References

Cowley, S. W. H. (1982), The causes of convection in the Earth's magnetosphere: A review of developments during the IMS, *Rev. Geophys.*, *20*(3), 531–565.

Lin, Y., and L. C. Lee (1994), Structure of reconnection layers in the magnetosphere, *Space Sci. Rev.*, *65*(1–2), 59–179.

Lin, Y., and X. Y. Wang (2005), Three-dimensional global hybrid simulation of dayside dynamics associated with the quasi-parallel bow shock, *J. Geophys. Res.*, *110*, A12216, doi:10.1029/2005JA011243.

Lockwood, M., T. G. Onsager, C. J. Davis, M. F. Smith, and W. F. Denig (1994), The characteristics of the magnetopause reconnection X-line deduced from low-altitude satellite-observations of cusp ions, *Geophys. Res. Lett.*, *21*(24), 2757–2760.

Newell, P. T., W. J. Burke, C. I. Meng, E. R. Sanchez, and M. E. Greenspan (1991), Identification and observations of the plasma mantle at low altitude, *J. Geophys. Res.*, *96*(A1), 35–45.

Newell, P. T., S. Wing, and F. J. Rich (2007), Cusp for high and low merging rates, *J. Geophys. Res.*, *112*, A09205, doi:10.1029/2007JA012353.

Onsager, T. G., C. A. Kletzing, J. B. Austin, and H. Mackiernan (1993), Model of magnetosheath plasma in the magnetosphere: Cusp and mantle particles at low-altitudes, *Geophys. Res. Lett.*, *20*(6), 479–482.

Onsager, T. G., S. W. Chang, J. D. Perez, J. B. Austin, and L. X. Janoo (1995), Low-altitude observations and modeling of quasi-steady magnetopause reconnection, *J. Geophys. Res.*, *100*(A7), 11,831–11,843.

Reiff, P. H., T. W. Hill, and J. L. Burch (1977), Solar-wind plasma injection at dayside magnetospheric cusp, *J. Geophys. Res.*, *82*(4), 479–491.

Rosenbauer, H., H. Grunwaldt, M. D. Montgomery, G. Paschmann, and N. Sckopke (1975), Heos 2 plasma observations in distant polar magnetosphere: The plasma mantle, *J. Geophys. Res.*, *80*(19), 2723–2737.

Shelley, E. G., R. D. Sharp, and R. G. Johnson (1976), Satellite-observations of an ionospheric acceleration mechanism, *Geophys. Res. Lett.*, *3*(11), 654–656.

Swift, D. W. (1996), Use of a hybrid code for global-scale plasma simulation, *J. Comput. Phys.*, *126*(1), 109–121.

Tan, B., Y. Lin, J. D. Perez, and X. Y. Wang (2011), Global-scale hybrid simulation of dayside magnetic reconnection under southward IMF: Structure and evolution of reconnection, *J. Geophys. Res.*, *116*, A02206, doi:10.1029/2010JA015580.

Trattner, K. J., J. S. Mulcock, S. M. Petrinec, and S. A. Fuselier (2007), Probing the boundary between antiparallel and component reconnection during southward interplanetary magnetic field conditions, *J. Geophys. Res.*, *112*, A08210, doi:10.1029/2007JA012270.

Wang, X. Y., Y. Lin, and S. W. Chang (2009), Hybrid simulation of foreshock waves and ion spectra and their linkage to cusp energetic ions, *J. Geophys. Res.*, *114*, A06203, doi:10.1029/2008JA013745.

Y. Lin, J. D. Perez, B. Tan, and X. Y. Wang, Physics Department, Auburn University, 206 Allison Lab., Auburn, AL 36849-5311, USA. (ylin@physics.auburn.edu; perez@physics.auburn.edu; tanbiny@auburn.edu; xywang@physics.auburn.edu)